1998

Simulating Gas at High Redshift

N Katz
University of Massachusetts - Amherst

L Hernquist

DH Weinberg

Simulating Gas at High Redshift

Neal Katz

Department of Physics and Astronomy, University of Massachusetts, Amherst, MA 01003

Lars Hernquist

Lick Observatory, University of California, Santa Cruz, CA 95064

David H. Weinberg

Department of Astronomy, The Ohio State University, Columbus, OH 43210

Abstract. We discuss simulations of gas at high redshift. We briefly review the methods used and the results for quasar absorption lines. We present gas mass functions and galaxy correlation functions for 5 different cosmological models. Galaxies should be detectable at redshifts greater than 2 by SKAI, and measurements of the gas mass functions and galaxy correlation functions could be used to discriminate between different cosmological models.

1. Introduction

Given all the talks in this conference about proposed telescopes to detect gas at high redshifts it is comforting as a theorist to think that here is an area where the theory might be ahead of the observations for a change. With the development of sophisticated computer codes and high performance computers it is now possible to model *ab initio* theories of structure formation with enough accuracy to make detailed predictions. In particular, unlike the computer simulations of the last decade, it is now possible to model the gas directly, including many important physical effects such as radiative cooling and heating by a photoionizing background field.

The latter effect is particularly important when modeling the Lyα forest. After all, observations of quasar absorption lines are observations of gas at high redshift, albeit at optical not radio or mm wavelengths. As we will discuss in this paper, it is our success in matching the observations of quasar absorption lines that gives us the confidence to extend our work to predicting radio and mm emission from high redshift gas. Before proceeding to the following sections, where we describe the methods used in the simulations, the simulations themselves, comparisons with observed quasar absorption lines, and possibilities for observing the gas in emission, we would like to quickly review some of the

basic questions we hope to answer by comparing theories with observations of gas at high redshifts.

What were the physical conditions of the primordial universe? What fraction of the matter was in a diffuse medium and what fraction in dense clouds? When did dense, neutral clouds first form? What fraction and types of dark matter were there? When and how did the formation of galaxies and large scale structure begin? How many metals were produced and how early? What was the typical background radiation field, how homogeneous was it, and what was producing it? Does the standard big bang model make the correct predictions about primordial element abundances?

2. Methods and Models

We perform our simulations using TreeSPH (Hernquist & Katz 1989), a code that unites smoothed particle hydrodynamics (SPH; Lucy 1977; Gingold & Monaghan 1977) with the hierarchical tree method (Barnes & Hut 1986) for computing gravitational forces. The collisionless matter and the gas are both represented by particles; collisionless particles are influenced only by gravity, while the gas is subject to gravitational forces, pressure gradients, and shocks. We include the effect of both radiative cooling, assuming primordial abundances, and Compton cooling. We also include the ionization and heat input from a UV radiation background under the optically thin assumption, using the field computed by Haardt & Madau (1996). Star formation is included heuristically to turn cold, dense gas into collisionless particles. Stars are allowed to form only in regions that are in convergent parts of the flow and that are locally Jeans unstable. Supernova heating is added to the remaining gas assuming a standard IMF from 0.1 to $100M_\odot$ and that stars above $8M_\odot$ become supernovae. Each supernova adds 10^{51} ergs of heat to the system. The method is described in detail in Katz, Weinberg, & Hernquist (1996).

Because it uses a Lagrangian hydrodynamics algorithm and individual particle time steps, TreeSPH can perform simulations with the enormous dynamic range essential for cosmological applications. To study high redshift galaxies such a large dynamic range is particularly important. In SPH, gas properties are computed by averaging or "smoothing" over a fixed number of neighboring particles, typically 30–100. When matter is distributed homogeneously, all particles have similar smoothing volumes. However, smoothing lengths in TreeSPH are allowed to decrease in collapsing regions, in proportion to the interparticle separation, thus increasing the spatial resolution in precisely those regions where a high dynamic range is needed. In underdense regions, the smoothing lengths are larger, but this is physically reasonable because the gas distribution *is* smoother in these regions, requiring fewer particles for an accurate representation. TreeSPH allows particles to have individual time steps according to their physical state, so that the pace of the overall computation is not driven by the small fraction of particles requiring the smallest time steps. The simulations presented here were performed using a highly vectorized but serial version of the code. We now have a version that runs on many parallel machines (Davé, Dubinski & Hernquist 1997), allowing us to perform even larger simulations in the future.

Here we present the results of 5 simulations of 5 different models. Each simulation, of a periodic cube that is $11h^{-1}$ Mpc on a side (where $h \equiv H_0/100\,\mathrm{km\,s^{-1}}$ Mpc^{-1}), uses 2×64^3 particles and is evolved to $z = 2$. Each has a nominal gas mass resolution (32 gas particles) of $4.7 \times 10^9 (\Omega_b/0.05)\,M_\odot$ and a spatial resolution (gravitational softening length, in physical units) of $6(1+z)^{-1}h^{-1}\,\mathrm{kpc}$. They all use $\Omega_b = 0.0125h^{-2}$ to satisfy the nucleosynthesis constraint (Walker et al. 1991).

The first model is "standard" CDM (SCDM), with $\Omega = 1$, $h = 0.5$. The power spectrum is normalized so that the rms amplitude of mass fluctuations in $8h^{-1}\,\mathrm{Mpc}$ spheres, linearly extrapolated to $z = 0$, is $\sigma_8 = 0.7$. This normalization is consistent with that advocated by White, Efstathiou & Frenk (1993) to match the observed masses of rich galaxy clusters, but it is inconsistent with the normalization implied by the COBE-DMR experiment. Our second model (CCDM) is identical to the first except that $\sigma_8 = 1.2$, consistent with the 4-year COBE data (Bennett et al. 1996). However, it produces rich clusters that are too massive. The third model, OCDM, assumes an open universe with $\Omega_0 = 0.4$, $h = 0.65$, and is also COBE-normalized (Ratra et al. 1997) and produces clusters of about the right mass. The fourth model, a nonzero-Λ CDM model (LCDM) has a tilted initial power spectrum to match both COBE and cluster masses. The fifth model (TCDM) is an $\Omega = 1$ model that also has a tilted initial power spectrum to match both COBE and cluster masses. The parameters of all the models are given in Table 1.

Table 1. Models

Model	Ω	Λ	H_0	Ω_b	σ_8	n
SCDM	1.0	0.0	50	0.05	0.7	1.0
CCDM	1.0	0.0	50	0.05	1.2	1.0
OCDM	0.4	0.0	65	0.03	0.75	1.0
LCDM	0.4	0.6	65	0.03	0.8	0.93
TCDM	1.0	0.0	50	0.05	0.54	0.80

3. The Simulations

At high redshift the gas ends up in three main components: low density, highly ionized gas with $\rho/\bar{\rho} \lesssim 10$ and $T \lesssim 10^5$ K, shock heated gas with typical overdensity $\rho/\bar{\rho} \sim 10$–10^4 and $T \sim 10^5$–10^7 K, and radiatively cooled, dense gas with $\rho/\bar{\rho} \gtrsim 1000$ and $T \sim 10^4$ K, as seen in the left panel of Figure 1. This panel shows the distribution of the gas particles in the temperature-density plane for SCDM at $z = 2$. The first component gives rise to the Lyα forest and follows the relationship $T = T_0(\rho/\bar{\rho})^\gamma$ with $T_0 \approx 6000$ K and $\gamma \approx 0.6$, as shown in the right panel of Figure 1. The second component is associated with galaxy halos, Lyman limit and metal line systems, and intracluster gas, while the third component is associated with damped Lyα systems and high redshift galaxies.

We can use the simulations to make artificial absorption spectra (Hernquist et al. 1996) to compare with the observations. "Typical" low column density absorbers — to the extent that we can identify such a class — are flattened structures of rather low overdensity ($\rho/\bar{\rho} \sim 1 - 10$), and have b-parameters that

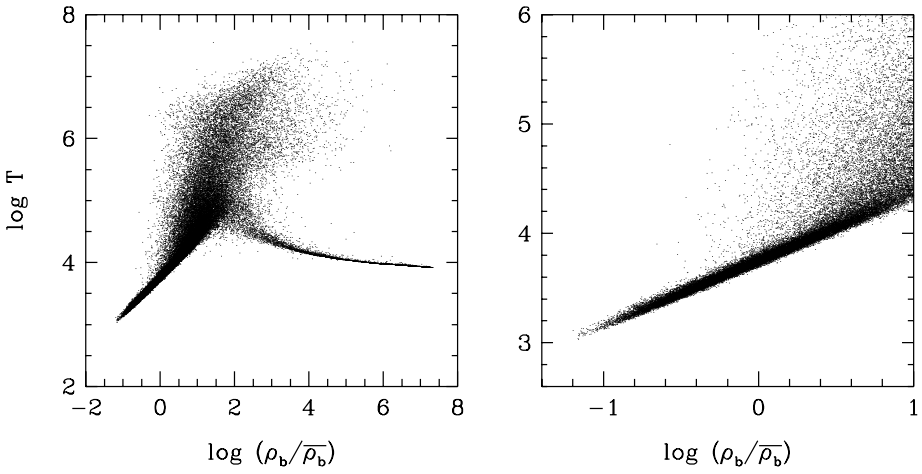

Figure 1. The distribution of gas particles in the temperature-density plane.

are often set by peculiar motions or Hubble flow rather than thermal broadening. Many systems are still expanding with residual Hubble flow, so their physical densities and neutral fractions decrease with time. The evolution of the Lyα forest is driven primarily by the increase in physical density with z, which raises the neutral fraction, and hence the opacity, of individual absorbers. Traditional searches for the Gunn-Peterson effect implicitly assume a uniform intergalactic medium (IGM) punctuated by discrete clouds; thus, absorption in identified lines is removed before seeking a continuum depression. The simulations reveal a smoothly fluctuating IGM, with no sharp distinction between "background" and "Lyα clouds". One might even say that the Lyα forest *is* the Gunn-Peterson effect. The Lyα forest contains most of the baryons in the Universe at $z = 2-5$.

As seen in Figure 2, for the SCDM model, the number of absorption systems matches the observations for systems with column densities from $10^{12.5}$ cm^{-2} to 10^{17} cm^{-2} (Hernquist et al. 1996; Davé et al. 1997). Davé et al. (1997) also show that the velocity widths of the Lyα absorbers match the observed distribution of line widths. All the models presented here also match these observations. The "standard" cold dark matter model and some of its variants can also naturally explain the associated HeII absorption (Croft et al. 1997) and metal-line absorption (Hellsten et al. 1997).

The high column density systems are associated with galaxies. Damped Lyα absorbers, $N \geq 10^{20.2}$ cm^{-2}, are lines of sight that pass near normal galaxies. Lyman limit absorbers (10^{17} cm$^{-2} \leq N \leq 10^{20.2}$ cm^{-2}) are lines of sight that pass through the halos of normal galaxies or near small dwarf galaxies. After a correction is made for self shielding, the number of high column density absorption systems in the SCDM model matches the observations for systems $> 10^{20}$ cm^{-2} (Katz et al. 1996; Gardner et al. 1997ab). The CCDM, OCDM, and LCDM models are roughly consistent with the observed damped Lyα abun-

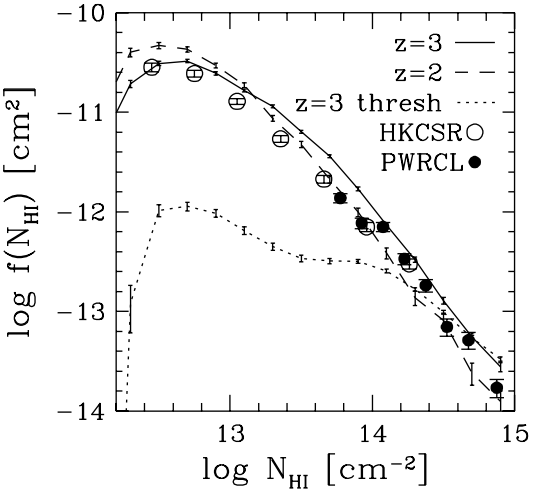

Figure 2. The column density distributions $f(N_{HI})$, the number of lines per unit redshift per linear interval of HI column density. Solid and dashed lines show the simulation results at $z = 3$ and $z = 2$, respectively. Filled and open circles show the observational results of Petitjean et al. (PWRCL;1993) and Hu et al. (HKCSR;1995), respectively. From Davé et al. (1997).

dance, but the TCDM model has too little small scale power and fails to produce enough damped absorption.

In the future, we plan to make more detailed comparisons with observations. In particular, we plan to analyze the simulated and observed spectra in the same exact way and compare the $f(N)$'s, b's, and line coincidences along closely spaced lines of sight. We plan to investigate the effects of our limited resolution, examine more cosmological models, and simulate the Lyα forest at low redshift.

Using the simulations we have shown that *ab initio* theories of structure formation, like CDM, make robust predictions and appear to match the properties of observed Lyα absorption systems. Hence, we can use the detailed physical state of the gas to calculate other observable properties of the gas.

In Figure 3 we plot the cumulative gas mass function of the galaxies in each of the five models at $z = 2$, 3, and 4. This mass does not include the stellar or dark matter components. We include all galactic gas whose temperature is less than $30,000$ K and whose overdensity is greater than 1000. We know that this approximately picks out the neutral HI gas owing to comparisons we made with calculations that used detailed but computationally expensive self-shielding corrections. The hydrogen fraction by mass in these simulations is 0.76, so the masses should be multiplied by this factor to get an upper limit to the HI masses. This is only an upper limit, since some of the hydrogen could be molecular. At first the mass function rises steadily towards lower redshift in all the models as more gas condenses into galaxies and small galaxies merge into larger systems. But then in the higher amplitude models, such as OCDM, CCDM, and SCDM, the mass function ceases to rise as the gas is converted into stars. In all cases the

flattening of the mass functions at $M_{gas} \lesssim 10^{9.5} M_{\odot}$ is a result of the simulations' finite mass resolution.

In Ingram et al. (1996) we "observed" simulations such as these with the Square Kilometer Array Interferometer (SKAI) to make artificial HI emission maps. We determined that the SKAI should detect about $10^{10}\, M_{\odot}$/beam in a 100 hour observation at the 5σ level. This can be compared to the galaxy gas masses in Figure 3. At these redshifts the beam should contain each galaxy. In several of the models, galaxies should be detectable by SKAI. By observing the gas mass function it may be possible to discriminate between different cosmological models.

Besides measuring the gas mass function of galaxies it should also be possible to measure the galaxy-galaxy correlation function. These are plotted for each model in Figure 4 at $z = 2$, 3, and 4. The solid lines are the correlation functions for the dark matter. As expected, the correlation functions of the dark matter rise towards lower redshift as structure grows in the universe. However, the correlation amplitude of the galaxies remains almost constant and in some cases even becomes smaller. This occurs because the galaxies are a highly biased population (Bagla 1997). The bias of the galaxies, which is proportional to the square root of the ratio of the correlation amplitude of the galaxies compared to that of the dark matter, ranges from 1.5 to 4 and is even higher when only the most massive galaxies are considered.

We plan to continue using the simulations to make detailed artificial HI maps, like those in Ingram et al. (1996), both to make testable predictions of the models and to help guide the construction of future large radio telescopes. We also plan to make artificial CO maps for comparisons with large mm telescopes such as the LMT.

Acknowledgments. We would like to thank Eric Linder for useful discussions. This work was supported by NASA grants NAG5-3525, NAG5-3922, and NAG5-4064.

References

Bagla, J.S. 1997, preprint (astroph/9711081)

Barnes, J.E. & Hut, P. 1986, Nature, 324, 446

Bennett, C., L., Banday, A. J., Gorskí, K. M., Hinshaw, G., Jackson, P., Keegstra, P., Kogut, A., Smoot, G. F., Wilkinson, D. T., Wright, E. L. 1996, ApJ, 646, L1

Croft, R.A.C., Weinberg, D.H., Katz, N., Hernquist, L., 1997, ApJ, 488, 532

Davé, R., Hernquist, L., Weinberg, D. H., & Katz, N., 1997, ApJ, 477, 21

Davé, R., Dubinski, J. & Hernquist, L. 1997, NewA, 2, 277

Gardner, J. P., Katz, N., Hernquist, L. & Weinberg D.H., 1997a ApJ484, 31

Gardner, J. P., Katz, N., Weinberg D.H. & Hernquist, L., 1997b ApJ486, 42

Gingold, R.A. & Monaghan, J.J. 1977, MNRAS, 181, 375

Haardt, F. & Madau, P. 1996, ApJ, 461, 20

Hellsten, U., Davé, R., Hernquist, L., Weinberg, D. H., & Katz, N. 1997, ApJ487 482

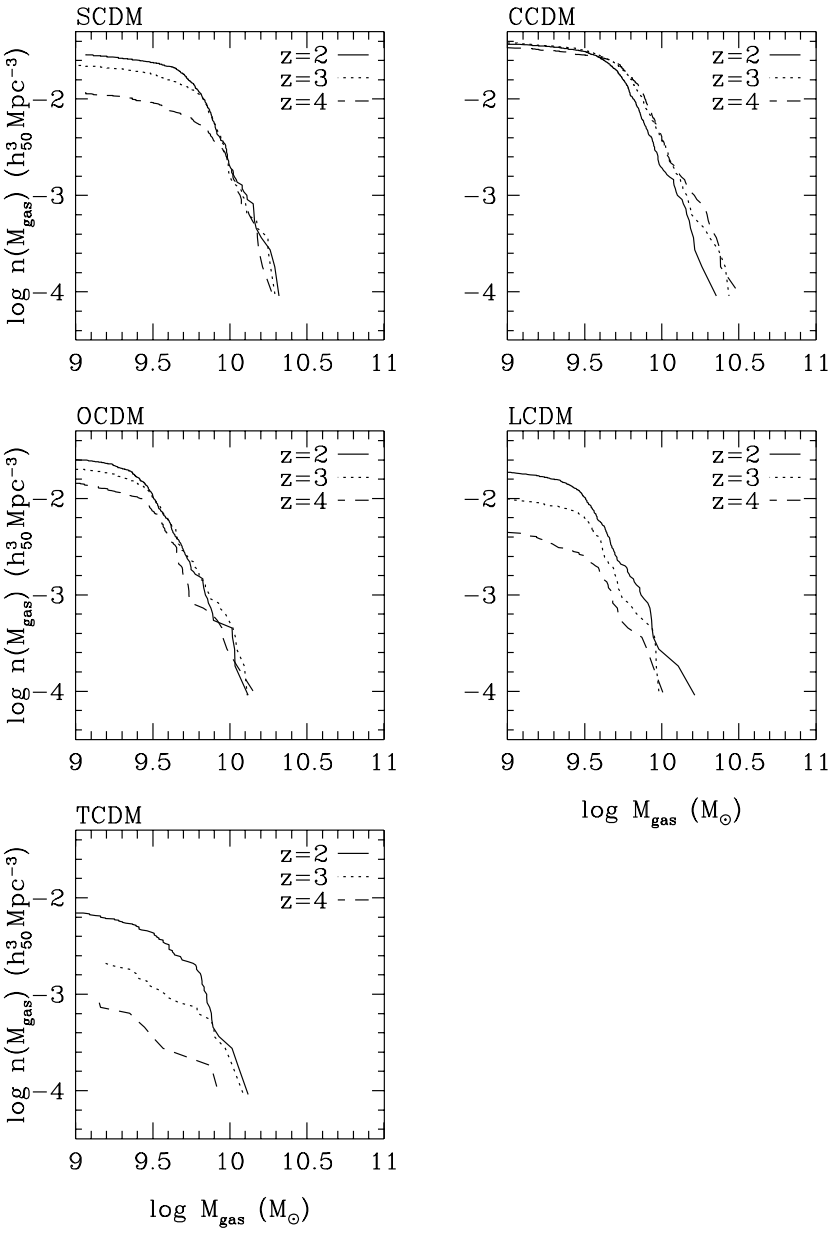

Figure 3. Cumulative gas mass function in the different models at the indicated redshifts: $n(M_{gas})$ is the comoving number density of galaxies whose gas mass exceeds M_{gas}.

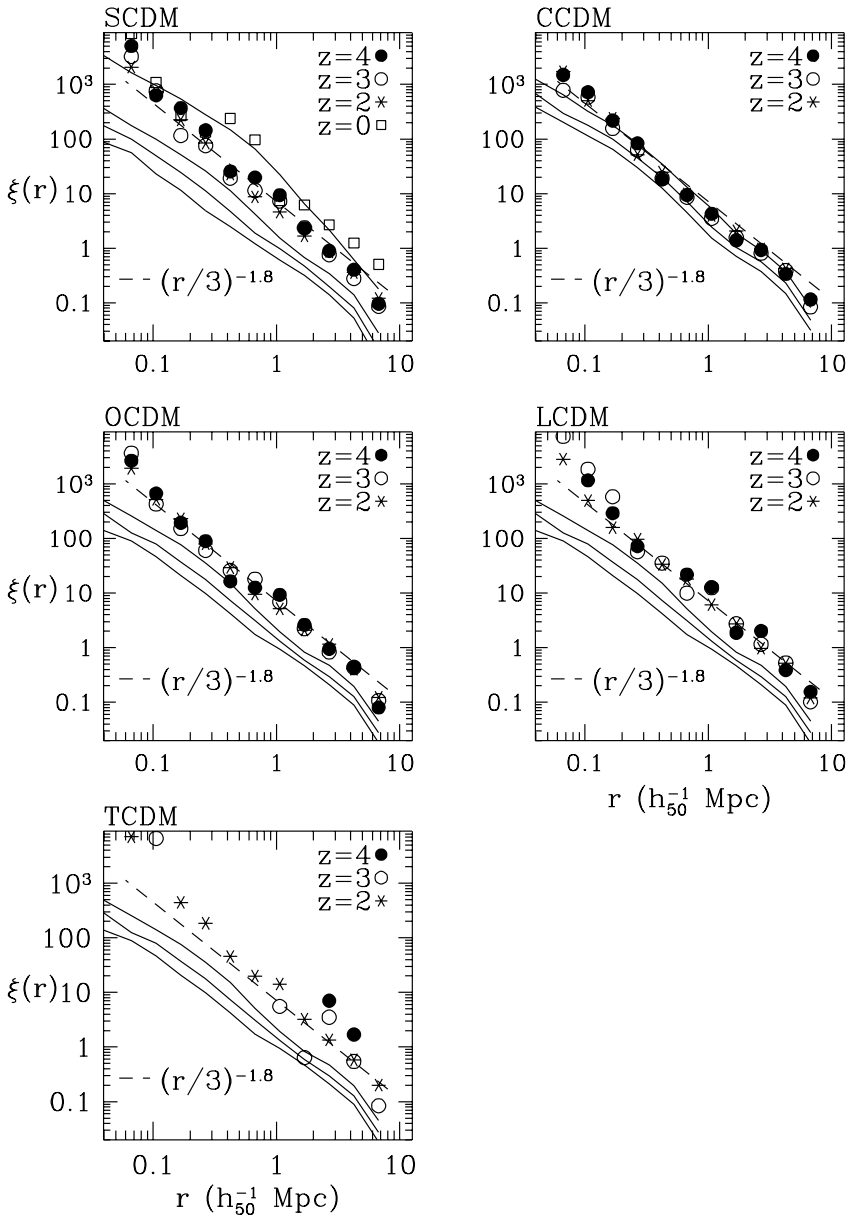

Figure 4. Symbols show the galaxy-galaxy correlation functions at the indicated redshifts. The solid lines are the correlation functions for the dark matter. The dashed line is a power law with a slope of -1.8 and a correlation length of 3 h_{50}^{-1} Mpc.

Hernquist, L. & Katz, N. 1989, ApJS, 70, 419

Hernquist L., Katz N., Weinberg D.H. & Miralda-Escudé J., 1996, ApJ, 457, L51

Hu, E.M., Kim, T.S., Cowie, L.L., Songaila, A & Rauch, M., 1995, AJ, 100, 1526

Ingram, D.R., Katz, N., Weinberg D.H. & Hernquist, L., 1996, in Cold Gas at High Redshift, M. Bremer, H. Rottgering, C. Carilli & P. van de Werf, Dordrecht: Kluwer Academic, 451

Katz, N., Weinberg, D.H. & Hernquist, L. 1996, ApJS, 105, 19

Katz N., Weinberg D.H., Hernquist, L. & Miralda-Escudé J., 1996, ApJ, 457, L57

Lucy, L. 1977, AJ, 82, 1013

Petitjean, P., Webb, J.K., Rauch, M., Carswell, R.F. & Lanzetta, K., 1993, MNRAS, 262, 499

Ratra, B., Sugiyama, N., Banday, A. J., & Gorski, K. M. 1997, ApJ, 481, 22

Walker T. P., Steigman, G., Schramm, D. N., Olive, K. A., Kang, H. S., 1991, ApJ, 376, 51

White, S. D. M., Efstathiou, G. P., & Frenk, C. S. 1993, MNRAS, 262, 1023